THE JOURNAL OF PHYSICAL CHEMISTRY B

Article

pubs.acs.org/JPCB

New Columnar Zn-Phthalocyanine Designed for Electronic Applications

Ivan H. Bechtold,*[,†,‡] Juliana Eccher,[†] Gregório C. Faria,[‡] Hugo Gallardo,[§] Fernando Molin,[§] Nicholas R. S. Gobo,[⊥] Kleber T. de Oliveira,[⊥] and Heinz von Seggern[‡]

[†]Departamento de Física, Universidade Federal de Santa Catarina—UFSC, 88040-900 Florianópolis, SC, Brazil

[‡]Department of Electronic Materials, Institute of Materials Science, Technical University of Darmstadt, Petersenstrasse 23, D-64287, Darmstadt, Germany

[§]Departamento de Química, INCT-Catálise, Universidade Federal de Santa Catarina—UFSC, 88040-900 Florianópolis, SC, Brazil

[⊥]Departamento de Química, Universidade Federal de São Carlos—UFSCar, 13565-905, São Carlos, SP, Brazil

Supporting Information

ABSTRACT: Columnar liquid crystals are composed of disk-shaped aromatic molecules surrounded by flexible side chains, where molecules self-assemble in columns and thereby form large surface-oriented domains. These systems are known for their good charge and exciton transport along the columns, with mobilities approaching those of aromatic single crystals. Such semiconducting materials are promising for devices applications, since the output efficiency can be tuned by properly aligning columns. In the work presented here, the synthesis and characterization of a new Zn-phthalocyanine (ZnPc) is described which exhibits remarkable properties, such as hexagonal columnar order, achieved by cooling down from the isotropic phase to room temperature. Such order was confirmed by optical microscopy and X-ray diffraction experiments. Diodes were constructed using spin-coated films, and the conductive properties were investigated by current versus voltage analysis, where mobilities of 10^{-3} and 10^{-2} $cm^2/(V\ s)$ were obtained for the nonannealed and annealed films, respectively.

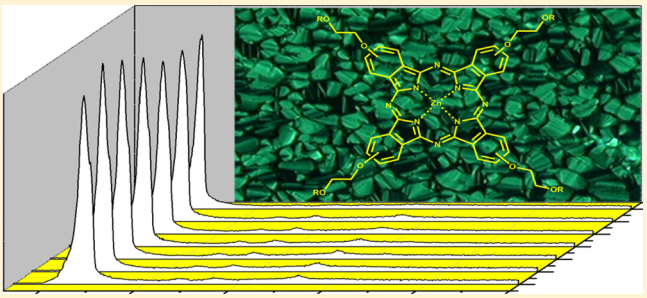

1. INTRODUCTION

Organic semiconductors with self-organizing properties, presented by liquid crystal materials, have been intensively explored for electronic applications in the past years. Many recent reports can be found in the literature discussing advantages of those ordered phases on organic light-emitting diodes (OLEDs), organic thin film transistors (OTFTs), and organic photovoltaics (OPVs). In all cases, the charge transport is strongly dependent on the degree of molecular order, which depends on the molecular structure as well as on the type of liquid crystalline order assumed by the system, which can be controlled through appropriate aligning methods.[1−4] For instance, rodlike molecules can pack in a layered arrangement, known as smectic phases, acting as 2D conductors in the plane of layers. Furthermore, disklike molecules pack as columnar structures, where short π-packing distance results in 1D conductors along the columns due to the efficient overlap of the π-orbitals of neighboring molecules, while the surrounding aliphatic chains act as a laterally isolating cladding.[5−7]

Many discotic molecules have been investigated for these purposes,[1,2] where the size and structure of the central core determine the local efficiency of the charge carrier transport due to the overlap of the π-orbital area. Meanwhile, longer aliphatic chains increase the insulating character around the columns, which avoid the intercolumnar tunneling of charge carriers. A balance between those factors contributes to the thermotropic behavior and the stabilization of the columnar mesophase. Usually, columnar order can be broken by heating the material above the clearing point, where the mesophase becomes isotropic. Recently, it was demonstrated that incorporation of an azo (N═N) linkage group in the central core of the disk allows the controlling of the columnar order, by a reversible *trans*−*cis*−*trans* photoisomerization process. A practical application could be an electronic device where the conduction properties are switched on or off by shining radiation of an appropriate wavelength and intensity.[8]

Phthalocyanines (Pc) are an interesting and important class of macrocyclic organic material that attracted considerable attention due to their potential for technological applications.[9,10] Those molecules are chemically and thermally stable and exhibit high absorption coefficients in the visible range. Pc derivatives may also present columnar liquid crystal phases with in-plane hexagonal order,[11−14] and have been applied in OTFTs and OPV devices. Dong et al.[15] demonstrated the

Received: August 7, 2012
Revised: October 4, 2012
Published: October 17, 2012

dx.doi.org/10.1021/jp307825u | *J. Phys. Chem. B* 2012, 116, 13554−13560

Scheme 1. Synthesis of ZnPc, Where Structure 3 Represents the Final Compound

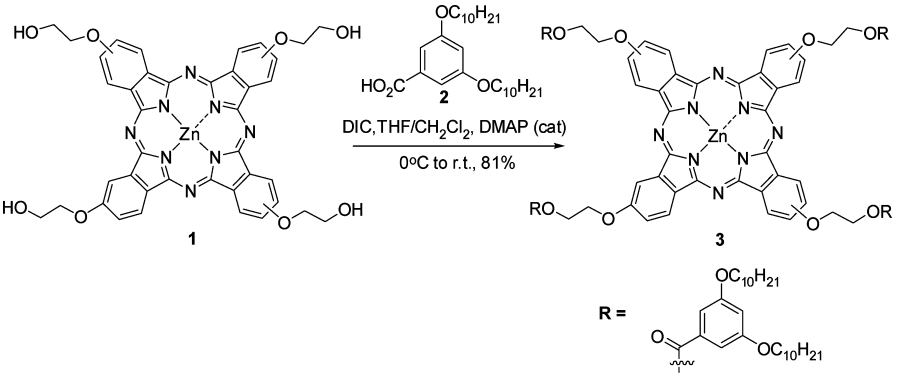

first solution-processed OTFTs using a vanadyl-complexed Pc with rectangular columnar structure, with mobilities higher than 0.017 $cm^2/(V\ s)$ on annealed spin-cast films. In the field of OPVs, ZnPc has been used as electron donor together with fullerene C_{60} acting as electron acceptor. In a recent achievement,[16] the fluorination of a ZnPc molecule to obtain F_4ZnPc was used to produce F_4ZnPc:C_{60} blends in a layered OPV device by vacuum deposition obtaining an efficiency of 4.6%. ZnPc was also synthesized with a linked C_{60} molecule.[17] Such system preserved a glassy liquid crystal state at room temperature after annealing, and exhibited ambipolar charge transport characteristics with similar mobilities of holes and electrons in the range of 10^{-2}–10^{-1} $cm^2/(V\ s)$ before and after annealing.

In the work presented here, the synthesis of a new ZnPc molecule is described, with small changes in the peripheral region of the disklike molecule. Thermal, structural, optical, and electronic properties of the final compound were evaluated. The current density versus voltage curves were analyzed in terms of an ohmic behavior for low voltages and a trap-controlled space-charge-limited charge transport through an exponential density of states for higher voltages.

2. EXPERIMENTAL SECTION

2.1. Measurements. ^{1}H NMR analysis was performed in a Bruker Avance 400 equipment using a mixture of deuterated chloroform ($CDCl_3$) and deuterated dimethyl sulfoxide (DMSO-d_6) as solvent (1:1) and tetramethylsilane (TMS) as internal standard (0.03%). The high-resolution mass spectrum was obtained using MALDI-TOF technique, AutoFlex Speed Bruker (laser 355 nm, 50 Hz) spectrometer, α-cyano-4-hydroxycinnamic acid as matrix, and Flex analysis as processing software.

The transition temperatures and associated enthalpy changes were determined by differential scanning calorimetry (DSC). The thermal stability was analyzed with a Shimadzu instrument with a DSC-50 and TGA-50 modules. A heating and cooling rate of 10 °C min^{-1} with a nitrogen flow of 50 mL min^{-1} was used. For the texture characterization, a small amount of powder was sandwiched between two glass slides, and a polarizing optical microscope (POM) (Olympus BX50) in transmission mode equipped with a Mettler Toledo FP82 hot stage to control the temperature was utilized. The images were recorded with a CCD camera coupled to the optical microscope.

The X-ray diffraction (XRD) experiments were carried out with the X'PERT-PRO (PANalytical) diffractometer using Cu Kα radiation (λ = 1.5418 Å) with an applied power of 1.2 kVA. The scans were performed in continuous mode from 2° to 30° (2θ angle) and the diffracted radiation was collected with the X'Celerator detector. The samples were prepared by heating up the powder material on a glass plate until the complete melting of the compound to the isotropic phase was achieved, followed by cooling to room temperature. As a result, a film of approximately 1 mm thickness was obtained. The film was then placed in the diffractometer chamber on a TCU2000 temperature control unit (Anton Paar), which allows a precise control of the sample temperature. During measurement the film was heated again to the isotropic phase and the diffraction patterns were collected while cooling through the mesophase.

The HOMO (highest occupied molecular orbital) and LUMO (lowest unoccupied molecular orbital) energy levels were obtained by cyclic voltammetry (CV), where the voltamogram was recorded at a scan rate of 100 mV s^{-1} from a solution of ZnPc (10^{-3} mol dm^{-3}) in dichloromethane in the presence of 0.1 mol tetrabutylammonium hexafluorophosphate ($TBAPF_6$) as supporting electrolyte. A three-electrode cell was used, comprising a glassy carbon electrode as the working electrode, a platinum wire as the counter electrode, an Ag^+/AgCl electrode as the reference, and the ferrocene/ferrocenium (Fc/Fc^+) redox couple as an internal standard. Before the measurement was started, the cell was deoxygenated by purging with nitrogen.

For the electrical analysis, diodes were fabricated using solution processing of the ZnPc in chloroform at a concentration of 10 mg/mL. ITO (indium tin oxide) coated glass plates with sheet resistances of about 15 Ω/□ were used as conductive substrates. After proper substrate cleaning, a thin layer of PEDOT:PSS was deposited by spin coating at 3000 rpm during 30 s, followed by annealing at 105 °C for 5 min. Then the ZnPc solution was spin-coated at 2000 rpm for 30 s. The thickness of the coated films was probed with a profilometer (Dektak 8000), and the morphology was determined by recording 256 × 256 lines with an atomic force microscope (Asilum Research) in tapping mode at scan rate of 0.8 Hz. Top electrodes were obtained by a sequential vacuum deposition (10^{-7} mbar) of Ca (20 nm) at 1 Å/s and Al (100 nm) at 2 Å/s. The active area of the diode was 9 mm^2. Devices were annealed at 260 °C, in order to achieve the ZnPc isotropic phase, followed by cooling to room temperature. The I/V curves were measured using a HP Semiconductor Parameter Analyzer (Model 4145A).

The UV–vis spectra of ZnPc were collected from a diluted chloroform solution and from spin-coated films using the

dx.doi.org/10.1021/jp307825u | J. Phys. Chem. B 2012, 116, 13554–13560

OceanOptics USB4000 spectrophotometer. In the latter case, films were coated onto quartz substrates.

2.2. Syntheses. Compounds **1** and **2** were synthesized according to the literature.[18,19] Compound **3** was prepared by an esterification of **1** through an activation of the carboxylic acid **2** with DIC (diisopropylcarbodiimide);[19] see Scheme 1. A mixture of Zn-phthalocyanine **1** (30.0 mg, 0.037 mmol) and 3,5-bis(decyloxy)benzoic acid (**2**) (95.1 mg, 0.220 mmol) was dissolved in 4 mL of CH_2Cl_2:THF (1:1) at 0 °C in nitrogen atmosphere. Catalytic amounts of *N*,*N*-dimethylaminopyridine (2 mg) and 46 μL of DIC (38 mg, 0.30 mmol) were added and the cooling was removed. The reaction was allowed to proceed at room temperature under darkness for 38 h. Thereafter, an additional excess of **2** (31.8 mg, 0.073 mmol) and DIC (38 mg, 0.30 mmol) were added and the reaction was stirred for additional 72 h. The solvent was removed and the product was purified by chromatography in silica gel (230−400 mesh) using dichloromethane/toluene/methanol (5:4:1) as eluent. Compound **3** was obtained in 81% yield after crystallization in methanol (73.6 mg, 0.030 mmol). ^{1}H NMR spectrum and MALDI-TOF of the final compound **3** are presented in Supporting Information (Figures S1 and S2).

3. RESULTS AND DISCUSSION

The thermal stability of ZnPc was evaluated by thermal gravimetric analysis (TGA) in order to determine the onset of thermal degradation, which is helpful to guide further phase transition investigations. The TGA curve demonstrated that an intense decomposition takes place only at temperatures above 390 °C.

The mesophase behavior of the ZnPc was determined by DSC, polarizing optical microscopy (POM), and XRD experiments. Figure 1 shows the DSC measurements for two

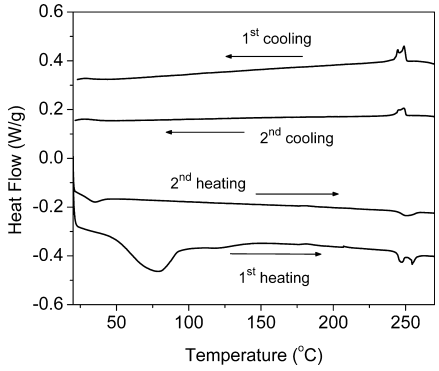

Figure 1. DSC results for two heating and cooling cycles, using a heating and cooling rate of 10 °C min^{-1} with a nitrogen flow of 50 mL min^{-1}.

cycles of heating and cooling. During the first heating cycle, clearly three endothermic transitions have been observed. The first transition is broad and centered around 75 °C. It is assumed that it is related to the transition from the crystal state to the liquid-crystal mesophase, where the asymmetry of the melting peak gives an indication of isomeric mixtures of ZnPc. The second and third peaks (between 245 and 254 °C) indicate two overlapping transitions, suggesting that in this temperature region the compound passes through different mesophase arrangements until achieving the isotropic liquid state. In the first cooling cycle from the isotropic liquid, the same two overlapping transitions are observed between 245 and 250 °C with some hysteresis. On the other hand, the intense recrystallization peak was not observed anymore; only a very weak transition seems to appear between 37 °C and room temperature. Further investigation of these two overlapping transitions by POM during heating and cooling does not indicate any textural changes. Due to the narrow temperature ranges in which those transitions occur, it was not possible to characterize them by XRD. In the second heating and cooling cycles the overlapping transitions close to the isotropic state are not evident; however, a small endothermic peak centered around 35 °C during the heating appears and the minor transition around 30 °C is again observed as in the first cooling cycle. The low enthalpy values associated with these transitions are consistent with a glassy liquid crystal state adopted by the system at room temperature.[16]

The textures of ZnPc as a function of temperature observed by POM are very similar to those described elsewhere.[20−22] Excellent textures of the compound were obtained by slowly cooling (5 °C min^{-1}) from the isotropic melt. A dendritic pattern was observed after the mesophase formation, by cooling down from the isotropic liquid state which coalesces to form a classical mosaic texture at 240 °C, typical of a columnar hexagonal mesophase (col_h) as can be seen in Figure 2a. It is possible to see that the col_h order persists until room temperature at 25 °C (Figure 2b).

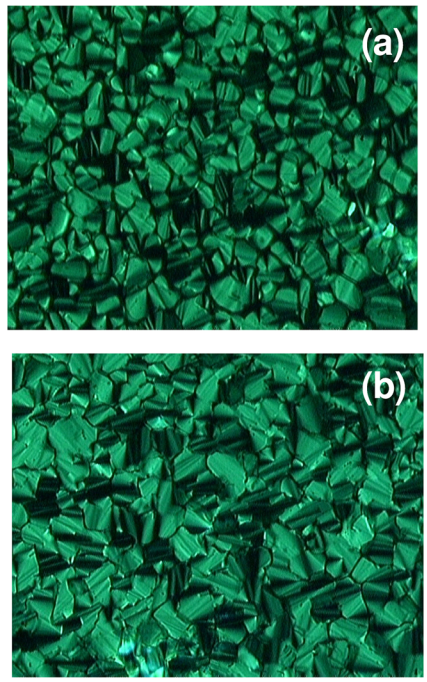

Figure 2. Optical micrographs of the ZnPc taken with POM at a magnification of 100×: (a) at 240 °C and (b) at room temperature (25 °C). Both textures are characteristic of a columnar hexagonal phase (col_h).

The mesophase assignments made by POM were ratified by XRD analysis. Figure 3a shows the diffraction pattern of ZnPc at 200 °C with indication of the associated Miller indices (100), (110), (200), (210), (300), and (220), which reflect the long-range intercolumnar ordering. The observed spacing values associated with those peaks were determined by applying the Bragg's law. The reciprocal spacing ratio obeys the relation $1:\sqrt{3}:\sqrt{4}:\sqrt{7}:\sqrt{9}:\sqrt{12}$, which is characteristic of hexagonal

dx.doi.org/10.1021/jp307825u | J. Phys. Chem. B 2012, 116, 13554−13560

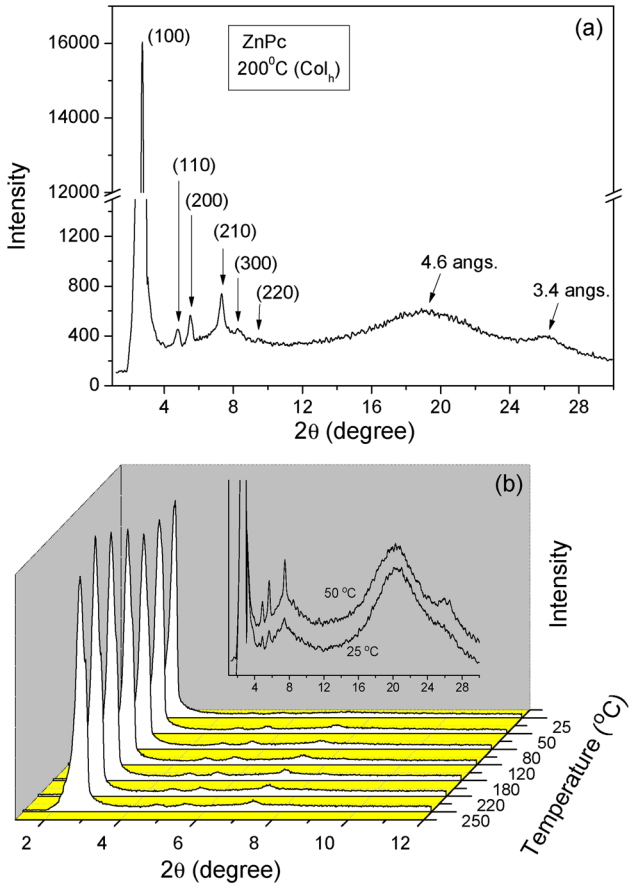

Figure 3. (a) XRD pattern of the hexagonal columnar mesophase of ZnPc at 200 °C. (b) Temperature dependence of the X-ray spectra; inset, the detail of 50 and 25 °C.

order.[23,24] The calculated spacing values were obtained by assuming the first maximum (100) and then the second-order peaks determined assuming a hexagonal structure, in order to compare with the measured values and to confirm the hexagonal phase.[25] The X-ray data are summarized in Table 1, where the lattice constant (a = 37.4 Å) was calculated from

Table 1. XRD Data of ZnPc at 200 °C

obsd spacings (Å)	calcd spacings (Å)	ratio	Miller indices	lattice const (Å)
32.4	32.4	1	100	a = 37.4
18.6	18.7	$\sqrt{3}$	110	
16.0	16.2	$\sqrt{4}$	200	
12.1	12.2	$\sqrt{7}$	210	
10.6	10.8	$\sqrt{9}$	300	
9.3	9.4	$\sqrt{12}$	220	
4.6				
3.4				

the position of the first maximum according to the equation $a = (2/3^{1/2})d_{10}$.[25] This result suggests a two-dimensional hexagonal lattice, where the disklike molecules are stacked in columns in a hexagonal arrangement.

The minimum and maximum diameters of the disklike ZnPc molecule were estimated to compare to the molecular diameter obtained from XRD data, which corresponds to the distance calculated for the first peak position (32.4 Å). For the diameter associated with the rigid ZnPc center using X-ray data from the literature,[26] a value of approximately 13 Å is obtained. For the most extended configuration of the lateral chains the ChemBio3D program was utilized, resulting in a value of approximately 54 Å for the maximum diameter. One can see that the diameter value measured in the mesophase fits in between the maximum and minimum diameters, indicating that the aliphatic chains are not in the most extended form and/or that there is an interdigitation of the aliphatic chains of the molecules of the different columns.[27]

In the wide angle region the ZnPc shows a diffuse halo around 4.6 Å ($2\theta \approx 19.3°$), which indicates liquidlike ordered chains and a broad reflection at around 3.4 Å ($2\theta \approx 26.2°$), which corresponds to the interdisk distance in a one-dimensional molecular stack.[25] The appearance of this reflection indicates that the molecules are well ordered along the columns and it is consistent with the intermolecular periodicity associated with the discotic hexagonal mesophase. In addition, this characteristic is especially important to enhance the electronic conduction along the columns.

In order to confirm the DSC result, which suggests that the hexagonal order is preserved until room temperature during cooling from the isotropic phase, diffractograms are collected during this process. The spectra are presented in Figure 3b and indicate that the intercolumnar spacings are not affected from 250 to 25 °C. The absence of new peaks in the wide angle region for 50 and 25 °C supports the lack of crystallinity of the material at room temperature after annealing; see inset of Figure 4b. It is also possible to observe that the intensity of the

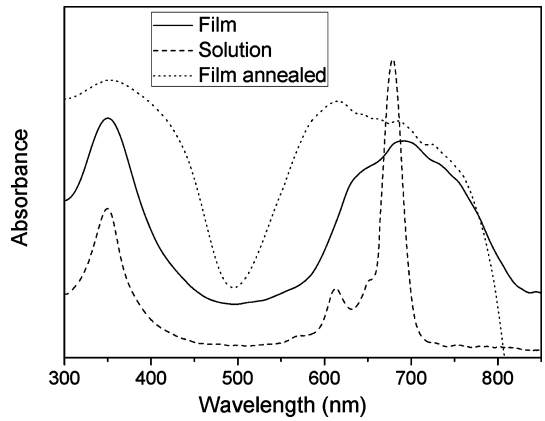

Figure 4. Absorbance of ZnPc at room temperature: thin spin-coated film (solid line), dilute chloroform solution (dashed line), and spin-coated film annealed until isotropic (dotted line). The spectra were adjusted for comparison and the measurements were performed at room temperature (25 °C).

broad reflection around 3.4 Å is reduced at 25 °C, suggesting that the interdisk order is slightly affected when the compound returns to room temperature. The same occurs for the intensity of the peaks in the low-angle region. This suggests a liquid crystal glassy state at room temperature with col$_h$ order and corroborates the DSC observations.

The UV−vis absorption spectra are presented in Figure 4. The spectrum in the UV−vis region of the ZnPc in solution is characteristic of metallophthalocyanines.[13] In solid films the peaks in the red region become broader, which is consistent with the aggregation of the molecules in the film. After annealing, a blue shift is observed, which supports the stacking of the disks in a columnar structure.[17] It is important to

dx.doi.org/10.1021/jp307825u | J. Phys. Chem. B 2012, 116, 13554−13560

emphasize that the strong absorption between 550 and 800 nm is a characteristic that makes ZnPcs attractive for OPV applications.

The device structure used for electrical characterization was ITO/PEDOT:PSS(45 nm)/ZnPc(60 nm)/Ca(20 nm)/Al(100 nm). The thicknesses of the PEDOT:PSS (45 nm) and ZnPc (60 nm) were determined by a profilometer, and the mean surface roughness (rms) for 15 μm × 15 μm images were 0.8 and 0.3 nm, respectively. It is worth mentioning that such surfaces were adequately smooth for technological applications. The electrical measurements were performed at room temperature in a controlled N_2 atmosphere. The current−voltage (I/V) and luminance−voltage characteristics of the ZnPc before (circles) and after annealing the diode at 260 °C (triangles) are presented in Figure 5. The results show a diodelike behavior,

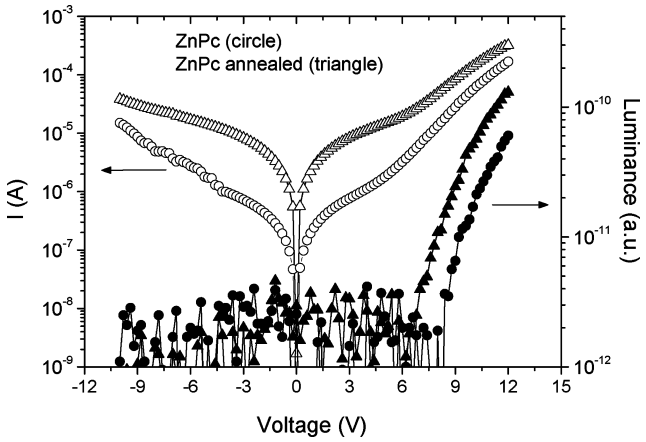

Figure 5. Current (left) and luminance (right) versus voltage for spin-coated films of ZnPc in a diode structure. Triangles and circles represent the annealed and nonannealed samples, respectively.

with a turn-on voltage at +6.6 V and +8.2 V for the annealed and nonannealed samples, respectively. However, a low degree of rectification is observed for both I/V curves. Following the procedures in refs 28,29, the LUMO has been determined to be at an energy level of −3.4 eV from CV measurements (see Figure S3 in the Supporting Information) and the band gap to be E_{gap} = 1.5 eV from the absorption spectra. Therefore, the HOMO has the value of −4.9 eV. These values are consistent with the literature values of ZnPc compounds.[17,30,31] Taking into account the energy diagram for our sample structure, one might expect a higher degree of rectification than that observed here. This effect could be related to any kind of chemical dopants in the compound. Nonrectifying current−voltage curves for ZnPc derivative compounds have been published previously.[32]

In Figure 5 the current density is higher for the annealed sample throughout the entire measurement, which is probably related to the higher mobility of that sample, due to the organization induced by the columns in the hexagonal phase. Both samples show a very low electroluminescence in the positive bias region. This can be related to the quenching of excitons near the Ca electrode due to the fact that in ZnPc the hole mobility is dominant.[17,33] The absence of electroluminescence on the reverse bias suggests the lack of one type of charge carrier in the diode. It is worth mentioning that the turn-on voltage difference between the annealed and nonannealed samples (6.6 and 8.2 V, respectively) suggests that injection and charge carrier transport is improved by the thermal treatment, which induces an improved organized structure in the active film.

Figure 6a shows the current density (J) versus voltage in a log−log plot, where a conduction regime following a power law

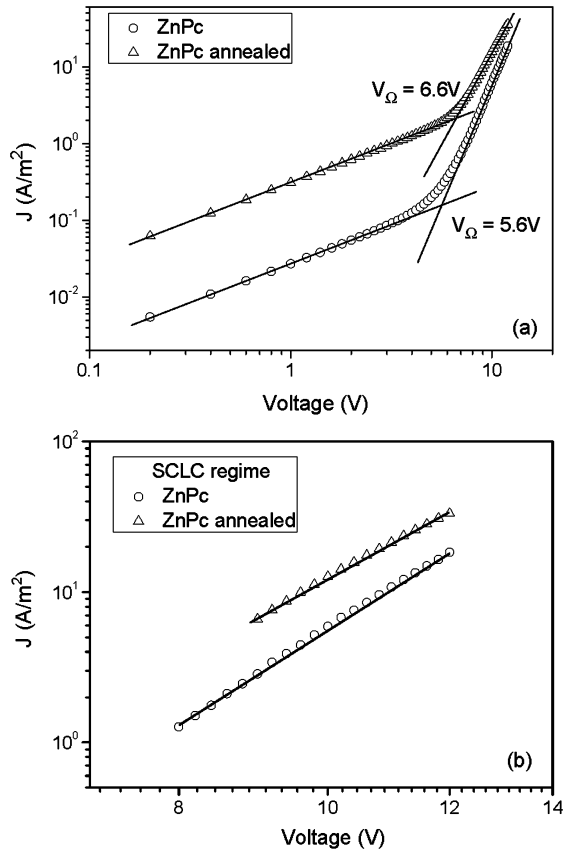

Figure 6. (a) Log−log plots of the $J \times V$ curves of the ZnPc films. Triangles and circles represent the annealed and nonannealed films, respectively. The solid lines serve as guides to determine the threshold voltages (V_Ω) between the two linear regimes; (b) SCLC region of both samples with subtraction of the ohmic regime from the curves of (a). The solid lines serve as guides to indicate the linear behavior.

$J \propto V^n$ is clearly evident for both the annealed and nonannealed samples. By applying a linear fit to the first regime (in the low-voltage region), a slope of n = 1 was obtained for both samples. On the other hand, a linear fit in the second regime resulted in values of $n > 2$ for both samples. The n = 1 regime indicates an ohmic behavior, which is consistent with the conduction of intrinsic thermally generated carriers inherent to the material, whereas the injected excess charge carriers dominate the $n > 2$ regime. From the intercept of the linear fits one can determine the transition voltage (V_Ω) between the two regimes, being equal to 6.6 and 5.6 V for the annealed and nonannealed samples, respectively. It is worth mentioning that for the annealed sample the value of V_Ω coincides with the turn-on voltage for electroluminescence, while for the nonannealed sample the turn-on voltage is 2.6 V higher than V_Ω. This indicates that for the annealed sample the voltage at which the injection current becomes dominant agrees with the voltage needed for the recombination of charge carriers. On the other hand, for the nonannealed film, even in the case when the injection current becomes dominant in the film above 5.6 V, light emission and therefore recombination sets in only for

dx.doi.org/10.1021/jp307825u | J. Phys. Chem. B 2012, 116, 13554−13560

Table 2. Physical Parameters Determined at Room Temperature for the Nonannealed and Annealed Films of ZnPc

sample	$l = n - 1$	μp_0 (m^{-1} V^{-1} s^{-1})	μH_t^{-1} (m^5 V^{-1} s^{-1})	μ (m^2 V^{-1} s^{-1})	H_t (m^{-3})
nonannealed	5.6	1.0×10^{10}	1.6×10^{-147}	1.0×10^{-7}	9.3×10^{24}
annealed	4.9	1.2×10^{11}	9.2×10^{-131}	1.2×10^{-6}	2.3×10^{25}

voltages exceeding 8.2 V. This behavior is likely to be associated with the organization of the columns induced by the annealing process. The data also showed that the ohmic behavior (in the low-voltage regime) is exactly the same for the positive and negative bias, which confirms that the conduction is dominated by intrinsic carriers. In addition, it is worth emphasizing that for high negative bias the ohmic transport dominates without the occurrence of space charge limited currents.

The second regime with a slope of $n > 2$ has already been related for ZnPc films to trap-controlled space-charge-limited conduction (SCLC) for an exponential distribution of trapping levels above the valence band.[33,34] To investigate the pure SCLC conduction, the ohmic behavior from the curves of Figure 6a must to be subtracted, which was not considered in refs 33 and 34. The result is shown in Figure 6b. For this subtraction, only the high-voltage regime >8 V is used to obtain reasonable signal-to-noise-ratios for the difference. For the slopes one obtains exponents for V of $n = 5.9$ and 6.6 for the annealed and nonannealed samples, respectively.

The physical parameters of the current−voltage curves were extracted and analyzed according to procedures well established in literature. For the first regime with $n = 1$, the relation between J and V can be given by the following equation

$$J = \frac{e\mu p_0 V}{d} \tag{1}$$

where e is the elementary charge, μ is the charge mobility, p_0 is the concentration of the thermally generated charges, and d is the thickness of the sample. From a comparison of the experimental results of Figure 6a and eq 1, one can uniquely obtain the product μp_0 as listed in Table 2.

For the SCLC regime, a single-carrier device is assumed, which seems justified by the weak light emission and the hole dominated transport reported for ZnPc. Lampert[35] considered the existence of an exponential trap distribution in the band gap of the form

$$H(E) = H_0 \exp(-E/kT_c) \tag{2}$$

where H_0 is the trap density per unit energy at the valence band edge, k Boltzmann's constant, and T_c a temperature parameter that describes the width of the trap distribution. In this case, the current density can be written as

$$J = e\mu N_v \left(\frac{\varepsilon\varepsilon_0}{eH_t}\right)^l \frac{V^{(l+1)}}{d^{(2l+1)}} \tag{3}$$

where N_v is the effective density of states, ε is the dielectric constant of the material, ε_0 is the vacuum permittivity, and $l = T_c/T$ correlates T_c with the temperature T of the sample. $H_t = H_0 kT_c$ is the total trap concentration in the exponential tail.[36] The values of T_c can be calculated directly from the experimentally obtained exponent $n = l + 1$ in the SCLC regime. By fitting the SCLC region in Figure 6b with eq 3, one is uniquely able to determine the value of the product μH_t^{-l}, as is listed in Table 2. In order to obtain the product, $N_v = 4 \times 10^{26}$ m^{-3} has been used which is determined from the number of molecules estimated from XRD data. Such density of states agrees well with published values of $N_v = 10^{27}$ m^{-3} normally used for organic materials.[37] In addition, the dielectric constant $\varepsilon = 2.0$ has been used for ZnPc.[32]

In order to estimate the physical parameters p_0 and H_t of the present system, values for the mobility were adapted from literature for similar ZnPc systems under comparable structural conditions, e.g., a charge carrier mobility for holes of 1.0×10^{-7} $m^2/(V\ s)$ for a nonannealed sample.[34] Under those assumptions the concentration of the thermally generated charges p_0 can be determined to be $p_0 = 1.0 \times 10^{17}$ m^{-3} and the total trap concentration H_t for the nonannealed sample assumes a value of $H_t = 9.3 \times 10^{24}$ m^{-3}. Both values are consistent with ref 34. Comparing the annealed sample to the nonannealed sample in Figure 6, one registers an increased current density for the annealed sample in both the ohmic regime Figure 6a and the SCLC regime Figure 6b. In the ohmic regime, the μp_0 product for the annealed sample is about 1 order of magnitude higher, which in principle can be related to variations of p_0 or μ or both. In the SCLC regime the increase in current density is about a factor of 2. Reports in the literature indicate an increase of the charge carrier mobility of annealed ZnPcs of about 1 order of magnitude due to the assumed columnar structure.[17] Due to these results, the increase of the current density in the ohmic regime between annealed and nonannealed samples is likely to be related to the increase of the charge mobility due to the organization of the columns. Under the assumption that there is no increase of p_0, the mobility of the annealed sample has increased to 1.2×10^{-6} $m^2/(V\ s)$. With this value of mobility, the total trap concentration can be calculated from the SCLC regime for the annealed sample. The result is listed in Table 2 and indicates a slight increase in trap density H_t. This result is unexpected due to the organization induced to the molecules; however, one explanation for this effect could be the generation of traps at boundaries between different columnar domains. At the same time, such an increase in trap density would reduce the number of delocalized states N_v which additionally reduces the current density in case of the SCLC compared to the ohmic regime. There are other effects that may reduce N_v such as the change in density of the annealed material, but such effects are considered to be small.

4. CONCLUSIONS

The synthesis and characterization of a new ZnPc molecule which exhibits a close packed columnar hexagonal mesophase after annealing remaining stable even at room temperature are presented and discussed. The UV−vis results are characteristic for ZnPc systems and turn out to be advantageous for OPV applications. The solution processed films of ZnPc are homogeneous and smooth, which is essential for processing for electronic applications. A power law dependence $J \propto V^n$ was observed for the current−voltage characteristic, where n was equal to 1 for low voltages, indicating an ohmic behavior. This is consistent with the conduction of thermally generated charge carriers. For higher voltages the conduction is dominated by the injection of charge carriers from the electrodes, where the index $n > 2$ was interpreted in terms of a trap-controlled SCLC through an exponential distribution of trapping levels above the

dx.doi.org/10.1021/jp307825u | J. Phys. Chem. B 2012, 116, 13554−13560

valence band. This approach explains the measured data very well, and the obtained parameters are comparable with those for similar ZnPc compounds in the literature. It is important to emphasize that after heating the films to the isotropic liquid state, followed by cooling to room temperature, the mobility increases by 1 order of magnitude, which was associated with the molecular order of the columnar hexagonal arrangement achieved by the thermal treatment. The mobilities of 10^{-7} and 10^{-6} $m^2/(V\ s)$ for the nonannealed and annealed film, respectively, are satisfactory for solution processed spin-coated ZnPc films. Finally, this compound seems to be promising for applications in OPVs, but further studies are necessary to reduce the high ohmic conduction to increase the rectifying ratio. In addition, the incorporation of electron acceptors like C_{60} or the preparation of blends is necessary to obtain bulk donor−acceptor heterojunctions.

■ ASSOCIATED CONTENT

Supporting Information

In Figure S1 we present the ^{1}H NMR spectrum and analysis of the final compound **3** (ZnPc). The MALDI-TOF characterization of the ZnPc is presented in Figure S2. In Figure S3 we show the CV measurement. This material is available free of charge via the Internet at http://pubs.acs.org.

■ AUTHOR INFORMATION

Corresponding Author

*E-mail: bechtold@fsc.ufsc.br. Tel.: ++55 48 3721-9234. Fax: ++55 48 3721-9946.

Notes

The authors declare no competing financial interest.

■ ACKNOWLEDGMENTS

The authors thank the following institutions for financial support: CAPES, CNPq, INCT/INEO, INCT-Catálise, PRONEX/FAPESC, and FAPESP. The XRD experiments were carried out in the Laboratório de Difração de Raios-X (LDRX-CFM/UFSC). Thanks are also due to Prof. Edson R. Filho and Marília A. Trapp for the MALDI-HRMS analysis.

■ REFERENCES

(1) Pisula, W.; Zorn, M.; Chang, J. Y.; Müllen, K.; Zentel, R. *Macrom. Rapid Commun.* **2009**, *30*, 1179−1202.
(2) Kaafarani, B. R. *Chem. Matt.* **2010**, *23*, 378−396.
(3) O'Neill, M.; Kelly, S. M. *Adv. Mater.* **2011**, *23*, 566−584.
(4) Brunet, T.; Thiebaut, O.; Charlet, E.; Bock, H.; Kelber, J.; Grelet, E. *Europhys. Lett.* **2011**, *93*, 16004(1−6).
(5) Segeyev, S.; Pisula, W.; Geerts, Y. H. *Chem. Soc. Rev.* **2007**, *36*, 1902−1929.
(6) Bushby, R. J.; Kawata, K. *Liq. Cryst* **2011**, *38*, 1415−1426.
(7) Cristiano, R.; Gallardo, H.; Bortoluzzi, A. J.; Bechtold, I. H.; Campos, C. E. M.; Longo, R. L. *Chem. Commun.* **2008**, 5134−5136.
(8) Westphal, E.; Bechtold, I. H.; Gallardo, H. *Macromolecules* **2010**, *43*, 1319−1328.
(9) In *Phthalocyanines: Properties and Applications*; Leznoff, C. C., Lever, A. B. P., Eds.; VCH: Weinheim, Germany, 1989−1996; Vol. *1*−*4*.
(10) Armstrong, N. R. J. *Porphyrins Phthalocyanines* **2000**, *4*, 414−417.
(11) Eichhorn, H.; Bruce, D. W.; Wöhrle, D. *Adv. Mater.* **1998**, *10*, 419−422.
(12) Eichhorn, H. *J. Porphyrins Phthalocyanines* **2000**, *4*, 88−102.
(13) Yılmaz, F.; Atilla, D.; Ahsen, V. *Polyhedron* **2004**, *23*, 1931−1937.
(14) Atilla, D.; Aslıbay, G.; Gürek, A. G.; Can, H.; Ahsen, V. *Polyhedron* **2007**, *26*, 1061−1069.
(15) Dong, S.; Tian, H.; Song, D.; Yang, Z.; Yan, D.; Geng, Y.; Wang, F. *Chem. Commun.* **2009**, 3086−3088.
(16) Meiss, J.; Merten, A.; Hein, M.; Schuenemann, C.; Schäfer, S.; Tietze, M.; Uhrich, C.; Pfeiffer, M.; Leo, K.; Riede, M. *Adv. Funct. Mater.* **2012**, *22*, 405−414.
(17) Hayashi, H.; Nihashi, W.; Umeyama, T.; Matano, Y.; Seki, S.; Shimizu, Y.; Imahori, H. *J. Am. Chem. Soc.* **2011**, *133*, 10736−10739.
(18) Cristiano, R.; Westphal, E.; Bechtold, I. H.; Bortoluzzi, A. J.; Gallardo, H. *Tetrahedron* **2007**, *63*, 2851−2858.
(19) de Oliveira, K. T.; de Assis, F. F.; Ribeiro, A. O.; Neri, C. R.; Fernandes, A. U.; Baptista, M. S.; Lopes, N. P.; Serra, O. A; Iamamoto, Y. *J. Org. Chem.* **2009**, *74*, 7962−7965.
(20) Duro, J. A.; de la Torre, G.; Barbera, J.; Serrano, J. L.; Torres, T. *Chem. Mater.* **1996**, *8*, 1061−1066.
(21) Kroon, J. M.; Koehorst, R. B. M.; van Dijk, M.; Sanders, G. M.; Sudhcolter, E. J. R. *J. Mater. Chem.* **1997**, *7*, 615−624.
(22) Sleven, J.; Görller-Walrand, C.; Binnemans, K. *Mater. Sci. Eng., C* **2001**, *18*, 229−238.
(23) Omenat, A.; Barbera, J.; Serrano, J. L.; Houbrechts, S.; Persoons, A. *Adv. Mater.* **1999**, *11*, 1292−1295.
(24) Wen, C.-R.; Wang, Y.-J.; Wang, H.-C.; Sheu, H.-S.; Lee, G.-H.; Lai, C. K. *Chem. Mater.* **2005**, *17*, 1646−1654.
(25) Gallardo, H.; Ferreira, M.; Vieira, A. A.; Westphal, E.; Molin, F.; Eccher, J.; Bechtold, I. H. *Tetrahedron* **2011**, *67*, 9491−9499.
(26) Scheidt, W. R.; Dow, W. *J. Am. Chem. Soc.* **1977**, *99*, 1101−1104.
(27) Yang, C. W.; Hsia, T. H.; Chen, C. C.; Lai, C. K.; Liu, R. S. *Org. Lett.* **2008**, *10*, 4069−4072.
(28) Seguy, I.; Jolinat, P.; Destruel, P.; Farenc, J.; Mamy, R.; Bock, H.; Ip, J.; Nguyen, T. P. *J. App. Phys.* **2001**, *89*, 5442−5448.
(29) Hellström, S.; Zhang, F.; Inganäs, O.; Andersson, M. R. *Dalton Trans.* **2009**, 10032−10039.
(30) Gao, W.; Kahn, A. *Org. Elect.* **2002**, *3*, 53−63.
(31) Shen, L.; Xu, Y.; Meng, F.; Ruan, S.; Chen, W. *IEEE 2011 Conference Proceedings*; DOI: 10.1109/SOPO.2011.5780502.
(32) Reis, F. T.; Mencaraglia, D.; Oould Saad, S.; Séguy, I.; Oukachmih, M.; Jolinat, P.; Destruel, P. *Synth. Met.* **2003**, *138*, 33−37.
(33) Li, B.; Chen, J.; Yang, D.; Ma, D. *Semicond. Sci. Technol.* **2011**, *26*, 115006−115010.
(34) Saleh, A. M.; Hassan, A. K.; Gould, R. D. *J. Phys. Chem. Solids* **2003**, *64*, 1297−1303.
(35) Lampert, A. M. *Prog. Phys.* **1964**, *27*, 329−367.
(36) Gould, R. D.; Rahman, M. S. *J. Phys. D: Appl. Phys.* **1981**, *14*, 79−89.
(37) Sussman, A. *J. Appl. Phys.* **1967**, *38*, 2738−2748.